

# $^3P_2$ Superfluids Are Topological

Takeshi Mizushima,<sup>1</sup> Kota Masuda,<sup>2,3</sup> and Muneto Nitta<sup>4</sup>

<sup>1</sup>*Department of Materials Engineering Science, Osaka University, Toyonaka, Osaka 560-8531, Japan*

<sup>2</sup>*Department of Physics, The University of Tokyo, Tokyo 113-0033, Japan*

<sup>3</sup>*Theoretical Research Division, Nishina Center, RIKEN, Wako 351-0198, Japan*

<sup>4</sup>*Department of Physics, and Research and Education Center for Natural Sciences, Keio University, Hiyoshi 4-1-1, Yokohama, Kanagawa 223-8521, Japan*

(Dated: December 9, 2024)

We clarify the topology of the  $^3P_2$  superfluidity which is expected to be realized in the cores of neutron stars and cubic odd-parity superconductors. The phase diagram includes the unitary uniaxial/biaxial nematic phases and nonunitary ferromagnetic and cyclic phases. We here show that the low-energy structures of all the phases are governed by different types of topologically protected gapless fermionic excitations: Surface Majorana fermions in nematic phases, single itinerant Majorana fermion in the ferromagnetic phase, and a quartet of itinerant Majorana fermions in the cyclic phase. Using the superfluid Fermi liquid theory, we also demonstrate that dihedral-two and -four biaxial nematic phases are thermodynamically favored in the weak coupling limit under a magnetic field. The mass acquisition of surface Majorana fermions in nematic phases is subject to symmetry.

PACS numbers: 67.30.H-, 26.60.Dd, 74.20.Rp

*Introduction.*— The modern concept of matter based on topology has recently spread over diverse fields in condensed matter. Nontrivial topology embedded in bulk brings about topological quantization in transport and anomalous electromagnetic responses [1, 2]. The topological viewpoint has also shed light on the new facet of low-lying structure in unconventional superconductors and superfluids [3–10]. The key ingredient is Majorana fermions residing in the surface/interface. They behave as non-abelian anyons [11, 12] and possess Ising-like magnetic anisotropy [13–16]. The former is expected to be a key for realizing fault-tolerant quantum computation [17, 18], while the Ising character is a consequence of intertwining of topology and symmetry [16].

The purpose of this paper is to unveil topological superfluidity relevant for the high dense core of neutron stars or cubic odd-parity superconductors [19–21]. Neutron stars are unique astrophysical objects under extreme conditions, such as rapid rotation and high magnetic fields. Superfluidity of neutrons gives a key to explain long relaxation time observed in the sudden speed-up events of neutron stars [22–24]. The reconstruction of the low energy structure due to neutron superfluids considerably affects cooling mechanism through the neutrino emission. In addition, the recently observed cooling of the neutron star (Cassiopeia A) might be attributed to neutrino emission enhanced at the onset of superfluid transition [25–28]. The existence of neutron superfluid components may also explain the sudden changes of spin periods observed in pulsars [29, 30]. Therefore, the superfluidity is an indispensable ingredient for understanding the evolution of neutron stars.

The prediction of  $^3P_2$  superfluidity in neutron stars dates back to 1970 [31, 32]. The strong spin-orbit force between nuclei generates the short-ranged attractive  $^3P_2$

interaction and the high density induces the repulsive core in the  $^1S_0$  channel. Hence, the  $^1S_0 \rightarrow ^3P_2$  transition occurs at the critical density ( $\sim 10^{14}\text{g/cm}^3$ ) relevant for the interior of neutron stars [31–36]. As seen in Fig. 1(a), superfluid states subject to the total angular momentum  $J=2$  are classified into three phases [36–38]. The nematic phase preserves the time reversal symmetry (TRS), while the cyclic and ferromagnetic phases are non-unitary states with spontaneously broken TRS. We notice that some of  $^3P_2$  phases may be realized in cubic odd-parity superconductors [19–21].  $^3P_J$  and the higher partial wave pairing states have also been discussed in cold atoms [39, 40]. The richness of  $^3P_2$  order parameters brings about various types of massive/massless bosonic modes [41–43] and exotic topological defects, including spontaneously magnetized vortices, fractional, and non-abelian vortices [35, 44–47]. In contrast to “bosonic” excitations, there have been no studies on the topology of “fermions” in  $^3P_2$  superfluids.

In this Letter, we clarify that various types of topologically protected fermions exist in  $^3P_2$  superfluids. The cyclic phase possesses eight Weyl points which form a quartet of itinerant Majorana fermions. In contrast, low-lying fermionic excitations in the nematic phase are governed by two-dimensional Majorana fermions emergent in the surface. Their mass acquisition in the nematic phase is prohibited by the intertwining of symmetry and topology. These observations on the topologically protected fermions may give a new insight into transports and cooling mechanism in the inner cores of neutron stars.

*Phase diagrams.*— We start to clarify the gap structure and the thermodynamic stability of  $^3P_2$  superfluid phases. The bulk states are determined by the Hamiltonian,  $\mathcal{H} = \frac{1}{2} \sum_{\mathbf{k}} \mathbf{c}^\dagger(\mathbf{k}) \mathcal{H}(\mathbf{k}) \mathbf{c}(\mathbf{k})$ . The Bogoliubov-de

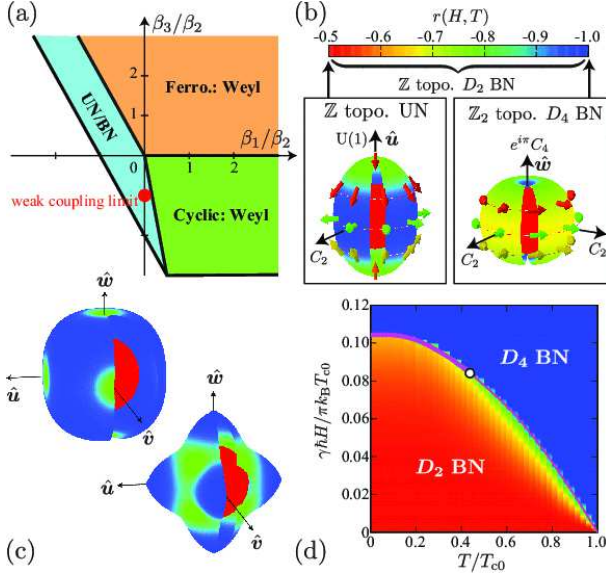


FIG. 1: (Color online) (a) Phase diagram obtained from the GL theory. (b) Gap and topological structures of nematic phases within  $r \in [-1, -\frac{1}{2}]$ , where the thick arrows represent the  $\mathbf{d}$ -vectors and the inner (red-colored) sphere denotes the Fermi sphere. (c) Gap structure of the upper (lower) band,  $E_+$  ( $E_-$ ), in the cyclic phase. (d) Phase diagram under a magnetic field, obtained from the quasiclassical theory. The thick (thin) curve denotes the first (second) order phase boundary.

Gennes (BdG) Hamiltonian density is given by

$$\mathcal{H}(\mathbf{k}) = \begin{pmatrix} \varepsilon(\mathbf{k}) & i\boldsymbol{\sigma} \cdot \mathbf{d}(\mathbf{k})\sigma_2 \\ i\sigma_2\boldsymbol{\sigma} \cdot \mathbf{d}^*(-\mathbf{k}) & -\varepsilon^T(-\mathbf{k}) \end{pmatrix}, \quad (1)$$

where  $\boldsymbol{\sigma}$  ( $\boldsymbol{\tau}$ ) is the Pauli matrices in spin (Nambu) spaces and  $\mathbf{c}^\dagger(\mathbf{k}) = [c_\uparrow^\dagger(\mathbf{k}), c_\downarrow^\dagger(\mathbf{k}), c_\uparrow(-\mathbf{k}), c_\downarrow(-\mathbf{k})]$  denotes the creation and annihilation operators in the Nambu space. The repeated indices imply the sum over (1, 2, 3). Here,  $\varepsilon(\mathbf{k})$  is composed of the  $2 \times 2$  single-particle Hamiltonian density subject to  $\text{SO}(3)_J$  and the magnetic Zeeman term  $-\gamma\hbar\mathbf{H} \cdot \boldsymbol{\sigma}/2$ . The  $^3P_2$  order parameter is given by the second-rank tensor,  $d_{\mu i}$ , where  $\mathbf{d}(\mathbf{k}) = d_{\mu i}\hat{k}_i$ . The quasi-particle excitation energy at zero fields is given by diagonalizing Eq. (1) as

$$E_\pm(\mathbf{k}) = \sqrt{\varepsilon_0^2(\mathbf{k}) + |\mathbf{d}(\mathbf{k})|^2 \pm |\mathbf{d}(\mathbf{k}) \times \mathbf{d}^*(\mathbf{k})|}, \quad (2)$$

where  $\varepsilon_0(\mathbf{k}) = \frac{1}{2}\text{tr}\varepsilon(\mathbf{k})$ . The Hamiltonian holds the particle-hole symmetry (PHS),  $\mathcal{CH}(\mathbf{k})\mathcal{C}^{-1} = -\mathcal{H}(-\mathbf{k})$ , with  $\mathcal{C} = \tau_1 K$ , where  $K$  is the complex conjugation operator. In addition, the TRS,  $\mathcal{T}\mathcal{H}(\mathbf{k})\mathcal{T}^{-1} = \mathcal{H}(-\mathbf{k})$  with  $\mathcal{T} = i\sigma_2 K$ , is preserved when  $d_{\mu i} \in \mathbb{R}$ .

The  $^3P_2$  order parameter,  $d_{\mu i}$ , reduces to the symmetric traceless tensor with five independent components. The ground state is determined by minimizing the Ginzburg-Landau (GL) energy functional  $\mathcal{F}$ , which is invariant under the simultaneous rotation of spin and orbital spaces,  $\text{SO}(3)_J$  and a gauge transformation,  $\text{U}(1)_\varphi$ .

The functional is given as  $\mathcal{F} = \alpha \text{tr}[dd^*] + \beta_1 |\text{tr}(dd^*)|^2 + \beta_2 [\text{tr}(dd^*)]^2 + \beta_3 \text{tr}[d^2 d^{*2}]$  [38]. Depending on  $\beta_i$ , there are three different phases as in Fig. 1. The nematic and cyclic order parameters are given as [36, 38, 48]

$$d_{\mu i} = \Delta(T, H) [\hat{u}_\mu \hat{u}_i + \mathcal{D} \hat{v}_\mu \hat{v}_i - (1 + \mathcal{D}) \hat{w}_\mu \hat{w}_i]. \quad (3)$$

in the basis of the orthonormal triad  $(\hat{\mathbf{u}}, \hat{\mathbf{v}}, \hat{\mathbf{w}})$ .

In the nematic phase,  $\mathcal{D}$  in Eq. (3) is specified by the real-valued parameter,  $r \in [-1, -1/2]$ , while the phase with  $\mathcal{D} = e^{i2\pi/3}$  is referred to as the cyclic phase. The former is the unitary state with the TRS, corresponding to highly degenerate minima of  $\mathcal{F}$  with respect to  $r$ . At  $r = -1/2$ ,  $d_{\mu i}$  is invariant under  $D_\infty = \text{SO}(2) \rtimes \mathbb{Z}_2 \simeq \text{O}(2)$  ( $\rtimes$  denotes a semi-direct product), which is called the uniaxial nematic (UN) phase. As shown in Fig. 1(b), the full gap with the hedgehog  $\mathbf{d}$ -vector is accompanied by the  $\text{U}(1)$  axis along  $\hat{\mathbf{w}}$  and  $C_2$  rotation axes in the  $\hat{\mathbf{u}}\text{-}\hat{\mathbf{v}}$  plane. The biaxial nematic (BN) phase at  $r = -1$  remains invariant under the dihedral-four  $D_4$  symmetry, which has one  $C_4$  and two  $C_2$  axes. The intermediate  $r$  holds the dihedral-two  $D_2$  symmetry with three  $C_2$  axes.

The cyclic phase is the nonunitary state which spontaneously breaks the TRS. As displayed in Fig. 1(c), this phase possesses two distinct bands composed of the full gap in  $E_+(\mathbf{k})$  and nodal gap in the  $E_-(\mathbf{k})$  branch. Another phase is known as the ferromagnetic phase, which is the eigenstate of  $J = M_J = +2$ ,  $d_{\mu i} = \Delta(\hat{u}_\mu + i\hat{v}_\mu)(\hat{u}_i + i\hat{v}_i)$ . This state is equivalent to the  $A_1$  phase of  $^3\text{He}$  [49], where neutrons with the spin  $\uparrow$  forms  $k_x + ik_y$  pairing, while the spin  $\downarrow$  neutrons remains in the normal state.

In Fig. 1(d), we display the phase diagram under a magnetic field, which is occupied by BN phases. This is obtained by minimizing the Luttinger-Ward thermodynamic potential with the superfluid Fermi liquid theory [50–53]. The magnetic field gives rise to the pair breaking in the momentum region within  $\mathbf{d} \cdot \mathbf{H} \neq 0$ . Consequently, the UN and  $D_2$  BN phases are always accompanied by the pair breaking because of  $\mathbf{d} \cdot \mathbf{H} \neq 0$  for any  $\mathbf{H}$ . The most favored configuration of  $\mathbf{d}$  under  $\mathbf{H}$  is  $\mathbf{d} \perp \mathbf{H}$ , which can be realized by only the  $D_4$  BN phase with the nodal direction aligned to  $\hat{\mathbf{w}} \parallel \mathbf{H}$ .

Two BN phases are separated by the second- (first-) order phase boundary in the higher (lower)  $T$  regime. The phase boundaries meet at the tricritical point at  $(T/T_{c0}, \gamma\hbar H/\pi k_B T_{c0}) = (0.45, 0.083)$ , where  $T_{c0}$  is the transition temperature at  $H = 0$ . In recent years, neutron stars having strong magnetic field  $H = 10^{13}\text{--}10^{15}$  G have been observed [54–57], where  $\gamma\hbar H/\pi k_B T_{c0}$  is estimated as 0.001–0.1 with  $T_{c0} = 0.2$  meV. The first-order phase boundary is sensitive to  $F_0^a$  that characterizes the magnetic response of the normal Fermi-liquid, and the region is enlarged (reduced) by negative (positive)  $F_0^a$ . This is attributed to the difference of the magnetic response. The  $D_2$  BN phase which has the hedgehog  $\mathbf{d}$ -vector suppresses the magnetization relative to that in the normal

state,  $|\mathbf{M}| < M_N$ , while the  $D_4$  BN phase with a two-dimensional configuration of  $\mathbf{d}$  shows  $|\mathbf{M}| = M_N$  when  $\hat{\mathbf{w}} \parallel \mathbf{H}$ . The effective magnetic field that neutrons experience is affected by the spin polarization of neutrons as  $H_\mu^{\text{eff}} = H_\mu - \frac{F_0^a}{1+F_0^a} \frac{M_\mu}{M_N}$ . Hence,  $\mathbf{H}^{\text{eff}}$  in the UN and  $D_2$  BN phases is always screened (enhanced) by the polarized medium for  $F_0^a < 0$  ( $F_0^a > 0$ ), and the enhancement/screening effect is fed back to the spin polarization of neutrons. In contrast, no enhancement/screening effect is realized in the  $D_4$  BN state and thus the spin polarization increases linearly on  $H$ .

Figure 1(a) is based on the weak coupling Fermi liquid theory, where no stable region of nonunitary states is found. However, strong coupling corrections that we omit here may support the stability of nonunitary states. The Fermi liquid behaviors of dense neutrons and strong coupling corrections were investigated in Refs. [58–62]. Similar to the  $A_1$  phase of the superfluid  $^3\text{He}$ , for instance, the Zeeman splitting of the Fermi surface in extremely high fields might favor the ferromagnetic phase.

*Cyclic phase.*— The cyclic phase possesses the exotic topological structure. As shown in Eq. (2), the nonunitary state has two distinct energy branches, where the upper (lower) branch  $E_+$  ( $E_-$ ) is fully gapped (gapless). One of eight point nodes in the  $E_-$  branch is identified as  $\mathbf{k}_0 = k_F(\hat{\mathbf{u}} + \hat{\mathbf{v}} + \hat{\mathbf{w}})/\sqrt{3}$ . The cyclic order parameter maintains the tetrahedral symmetry with three  $C_2$  axes along  $\hat{\mathbf{u}}$ ,  $\hat{\mathbf{v}}$ , and  $\hat{\mathbf{w}}$  and four  $C_3$  axes accompanied by the  $e^{i2\pi/3}$  phase rotation. As shown in Fig. 2(a), the symmetry guarantees that the point nodes exist at four vertices of the tetrahedron,  $\{\mathbf{k}_0, C_{2,u}\mathbf{k}_0, C_{2,v}\mathbf{k}_0, C_{2,w}\mathbf{k}_0\}$ . In addition, the PHS,  $\mathcal{CH}(\mathbf{k})\mathcal{C}^{-1} = -\mathcal{H}(-\mathbf{k})$ , implies that the point nodes must appear as a pair in the  $\mathbf{k}$ -space, e.g.,  $\mathbf{k}_0 \leftrightarrow -\mathbf{k}_0$ . Hence, the nodal positions are identified in terms of the label of vertices of the tetrahedron,  $\alpha$ , and the index  $q = \pm 1$  associated with the PHS partner as

$$\{\mathbf{k}_{q,\alpha}\}_{\alpha=1,\dots,4}^{q=\pm 1} = \{q\mathbf{k}_0, qC_{2,u}\mathbf{k}_0, qC_{2,v}\mathbf{k}_0, qC_{2,w}\mathbf{k}_0\}. \quad (4)$$

It is convenient to introduce the new triad  $(\hat{\mathbf{e}}_1, \hat{\mathbf{e}}_2, \hat{\mathbf{e}}_3)$ , where  $\hat{\mathbf{e}}_3 \equiv \hat{\mathbf{e}}_1 \times \hat{\mathbf{e}}_2$  is taken along the nodal direction  $\mathbf{k}_0$ , as shown in Fig. 2(a). Let  $V_{q,\alpha}$  be a small region around  $\mathbf{k}_{q,\alpha}$ . In the new basis and the region of  $\mathbf{k} \in V_{q,\alpha}$ , the  $4 \times 4$  BdG matrix is decomposed into a pair of the  $2 \times 2$  matrix,  $\mathcal{H}(\mathbf{k}) \mapsto \text{diag}[\mathcal{H}_+(\mathbf{k}), \mathcal{H}_-(\mathbf{k})]$  [50]. The branch of  $E_-(\mathbf{k})$  is given by  $\mathcal{H}_-(\mathbf{k})$  with the order parameter  $\bar{\Delta} \hat{\mathbf{e}}_+^\mu \hat{\mathbf{e}}_-^i$  which is the eigenstate of  $M_J = -2$ . The fully gapped branch,  $E_+(\mathbf{k})$ , is characterized by  $\mathcal{H}_+(\mathbf{k})$  with  $\bar{\Delta} \hat{\mathbf{e}}_+^\mu \hat{\mathbf{e}}_+^i$  which is the eigenstate of  $M_J = 1$ . We here introduced  $\hat{\mathbf{e}}_\pm = (\hat{\mathbf{e}}_1 \pm i\hat{\mathbf{e}}_2)/\sqrt{2}$  and  $\bar{\Delta} \equiv \Delta e^{i4\pi/3}$ . The low-energy effective Hamiltonian in the cyclic phase is therefore governed by  $\mathcal{H}_- = \sum_{q,\alpha} \sum_{\mathbf{k} \in V_{q,\alpha}} \mathbf{c}_\alpha^\dagger(\mathbf{k}) \mathcal{H}_-^{q,\alpha}(\mathbf{k}) \mathbf{c}_\alpha(\mathbf{k})$  with

$$\mathcal{H}_-^{q,\alpha}(\mathbf{k}) = \boldsymbol{\tau} \cdot \mathbf{g}(\mathbf{k} - \mathbf{k}_{q,\alpha}), \quad (5)$$

where  $\mathbf{g}(\mathbf{k}) = (\bar{\Delta} k_z/k_F, \bar{\Delta} k_y/k_F, qv_F k_z)$ ,  $\mathbf{k} = k_1 \hat{\mathbf{e}}_1 + k_2 \hat{\mathbf{e}}_2 + k_3 \hat{\mathbf{e}}_3$ , and  $\mathbf{c}_\alpha(\mathbf{k}) = [c_\alpha(\mathbf{k}), c_\alpha^\dagger(-\mathbf{k})]^T$ . Each point node

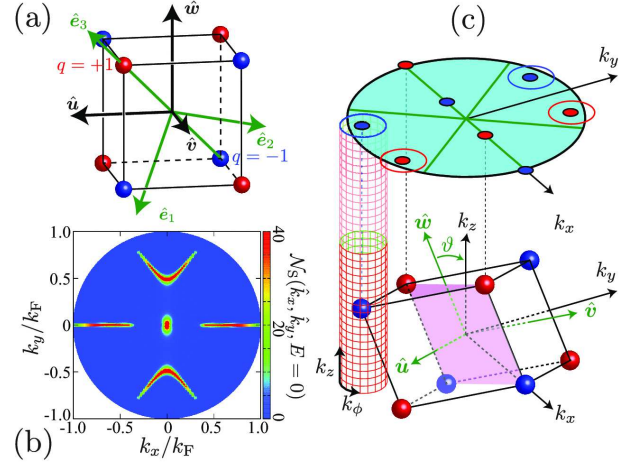


FIG. 2: (Color online) (a) Configuration of Weyl points,  $\{\mathbf{k}_{q,\alpha}\}$ , with monopole and antimonopole charges ( $q = \pm 1$ ) in the cyclic phase. (b) Momentum-resolved zero-energy density of states on the surface for the misorientation angle  $\vartheta = 2\pi/5$ . (c) Gap structure of the cyclic phase where Weyl points are projected to the surface momentum space  $k_x$ - $k_y$  (surface is normal to  $\hat{\mathbf{z}}$ ). The first Chern number is defined on the cylindrical surface enclosing a Weyl point, and the shaded area in the  $k_x$ - $k_z$  plane denotes  $P_2$  symmetric momenta.

at  $\mathbf{k}_{q,\alpha}$  is identified as the Weyl point by the monopole charge  $q_m = +1$  ( $q_m = -1$ ) for  $q = +1$  ( $-1$ ), which is a source of fictitious hedgehog-like magnetic field in  $\mathbf{k}$  space. Hence, the low-lying fermionic excitations behave as Weyl-type Bogoliubov quasiparticles, and the effective gauge field  $\mathbf{A}$  emerge as  $\mathbf{k}_{q,\alpha} = \mathbf{A}$ .

We now introduce the coordinate centered on the Weyl point,  $\mathbf{K} \equiv \mathbf{k} - \mathbf{k}_{q,\alpha}$ . The four-component real quantum field,  $\psi(\mathbf{r}) = \mathcal{C}\psi(\mathbf{r})$ , is constructed from a PHS pair of the single-species Weyl fermions as  $\psi_\alpha(\mathbf{r}) \equiv \sum_{\mathbf{K}} e^{i\mathbf{K} \cdot \mathbf{r}} \psi_\alpha(\mathbf{K})$  with  $[c_\alpha(\mathbf{K}), c_\alpha(\mathbf{K}), c_\alpha^\dagger(-\mathbf{K}), c_\alpha^\dagger(-\mathbf{K})]^T$  [63]. The low energy part of the Hamiltonian is governed by massless Majorana fermions

$$\mathcal{H} \approx \mathcal{H}_- = \sum_{\alpha=1}^4 \int d^3\mathbf{r} \bar{\psi}_\alpha(\mathbf{r}) [-i\bar{v}_\mu \gamma_\mu \partial_\mu] \psi_\alpha(\mathbf{r}), \quad (6)$$

where we introduced  $\bar{\psi} = (\tau_1 \psi)^T$ ,  $\bar{\mathbf{v}} = (\bar{\Delta}/k_F, \bar{\Delta}/k_F, v_F)$ , and  $\boldsymbol{\gamma} = (\mu_1 \tau_1, \mu_1 \tau_2, \mu_3)$  with the Pauli matrices  $\mu_i$  labeled by  $q = \pm 1$ . The itinerant Majorana fermions with pseudospin  $\frac{1}{2}$  form a quartet  $(\psi_1, \psi_2, \psi_3, \psi_4)$  as a consequence of the tetrahedral symmetry. We notice that the nonunitary ferromagnetic phase is accompanied by a single itinerant Majorana fermion with  $\uparrow$  spin.

Figure 2(b) shows the  $\mathbf{k}$ -resolved zero-energy density of states on the surface,  $\mathcal{N}_s(\hat{k}_x, \hat{k}_y, E=0)$  [50], where the surface normal axis  $\hat{\mathbf{z}}$  is assumed to be deviated from  $\hat{\mathbf{w}}$  by angle  $\vartheta$ . The zero energy states form the Fermi arc connecting the Weyl points projected onto the surface. We emphasize that the Fermi arc is protected by two different topological origins: The first Chern number (Ch<sub>1</sub>)



and the winding number protected by a hidden symmetry. For unitary states with a single pair of Weyl points, the Fermi arc appears as a consequence of  $\text{Ch}_1 \neq 0$  well-defined in a sliced two-dimensional momentum plane. In the cyclic phase, however, the energy dispersions always have the level crossing,  $E_+(\mathbf{k}) = E_-(\mathbf{k})$ , on  $\mathbf{k}$  along  $\hat{\mathbf{u}}$ ,  $\hat{\mathbf{v}}$ , and  $\hat{\mathbf{w}}$ .  $\text{Ch}_1$  is ill-defined on the plane which intersects the level-crossing lines. As displayed in Figs. 2(b) and 2(c), only four Weyl points at nonzero  $k_y$  have  $\text{Ch}_1 = 1$  on the cylindrical  $(k_\phi - k_z)$  surface which does not intersect the level-crossing lines, whereas the other Weyl points have no well-defined  $\text{Ch}_1$ .

To uncover the topological origin of the Fermi arc along the  $k_x$  axis, we first notice that  $\mathcal{H}(\mathbf{k})$  in the cyclic phase is invariant under the combined symmetry,  $P_2 = \mathcal{T}\mathcal{M}$ . The operator in the Nambu space,  $\mathcal{M} = \text{diag}(M, -M^*)$ , denotes the mirror reflection in the  $x$ - $z$  plane, and  $M$  changes  $\sigma \mapsto (-\sigma_x, \sigma_y, -\sigma_z)$  and  $\mathbf{k} \mapsto (k_x, -k_y, k_z)$ , respectively. Although the cyclic order parameter in Eq. (3) breaks  $\mathcal{T}$  and  $M$ , independently, it remains invariant under the combined symmetry,  $\mathcal{T}M\Delta(\mathbf{k})(\mathcal{T}M^*)^{-1} = -\Delta(-k_x, k_y, -k_z)$ . Combining it with the PHS, one obtains the chiral symmetry,  $\Gamma \equiv -i\mathcal{C}P_2$ , satisfying  $\{\Gamma, \mathcal{H}(k_x, 0, k_z)\} = 0$ . As long as the symmetry is maintained, the one dimensional winding number in the chiral symmetric momenta  $\mathbf{k} = (k_x, 0, k_z)$  is defined as the topological invariant relevant to the surface Fermi arc at  $k_y = 0$ ,

$$w_{1d}(k_x) = -\frac{1}{4\pi i} \int_{-\infty}^{+\infty} dk_z \text{tr}[\Gamma \mathcal{H}^{-1}(\mathbf{k}) \partial_{k_z} \mathcal{H}(\mathbf{k})], \quad (7)$$

which is estimated as  $w_{1d}(k_x) = 1$  for  $|k_x|/k_F \in [0.32, 1.0]$ . The chiral symmetry guarantees that all energy eigenstates are labeled by the eigenstates  $\Gamma = \pm 1$ .  $w_{1d}$  is identical to the difference in the number of zero-energy states in each chiral subsector,  $|w_{1d}| = |N_+ - N_-|$  [64]. In contrast to  $\text{Ch}_1$ , the Fermi arc is only protected by the  $P_2$  symmetry. A magnetic field misoriented from the mirror plane explicitly breaks the  $P_2$  symmetry and the Fermi arc along the  $k_x$  axis disappears.

*Majorana fermions in nematic phases.*— Although nematic phases are not accompanied by itinerant gapless fermions, localized gapless fermions exist in topological defects as a consequence of nontrivial topology. To clarify this, we first present the bound state solution of the BdG equation,  $\mathcal{H}(k_x, k_y, -i\partial_z)\varphi(\mathbf{r}) = E\varphi(\mathbf{r})$ , where  $\varphi(\mathbf{r})$  denotes the four-component wavefunction in the Nambu space. The surface is set to be normal to  $\hat{\mathbf{z}}$  and the specular boundary condition is imposed on  $\varphi$  as  $\varphi(x, y, 0) = 0$ .

In the absence of a time-reversal breaking field, surface bound fermions exist in the nematic phases, which have the anisotropic relativistic dispersion as  $E_0(\mathbf{k}_\parallel) = \pm \sqrt{c_x^2 k_x^2 + c_y^2 k_y^2}$ , where  $|E_0| < \Delta$ . The velocity reflects the orientation of the triad  $(\hat{\mathbf{u}}, \hat{\mathbf{v}}, \hat{\mathbf{w}})$  with respect to the surface. For  $\hat{\mathbf{u}} \parallel \hat{\mathbf{z}}$ , the velocities are  $c_x = \frac{\Delta_0}{k_F}$  and

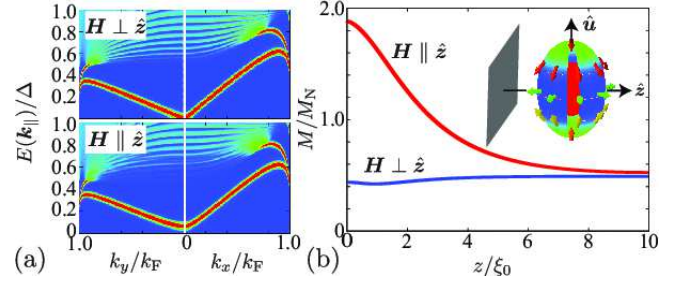


FIG. 3: (Color online) (a) Momentum-resolved surface density of states, and (b) local magnetization for  $\mathbf{H} \perp \hat{\mathbf{z}}$  and  $\mathbf{H} \parallel \hat{\mathbf{z}}$ , in the nematic phase with  $\hat{\mathbf{u}} \perp \hat{\mathbf{z}}$ .

$c_y = \frac{\Delta_0}{k_F} r(H)$ , while  $c_x = \frac{\Delta_0}{k_F}$  and  $c_y = \frac{\Delta_0}{k_F} [1 + r(H)]$  for  $\hat{\mathbf{u}} \perp \hat{\mathbf{z}}$ . The gapless surface fermions having a cone-shaped dispersion exist in the case of  $r \neq -1$ . The quantized field constructed from such gapless state obeys the Majorana condition [50]  $\psi_\uparrow = i\psi_\downarrow^\dagger$ . The effective Hamiltonian for surface bound states is given with the two-component spinor  $\psi = (\psi_\uparrow, \psi_\downarrow)$  and  $\bar{\psi} = i(\sigma_1 \psi)^\text{T}$  as,  $\mathcal{H}_{\text{surf}} = \int d^2\mathbf{r}_\parallel \bar{\psi}(\mathbf{r}_\parallel) (-i\bar{v}_\mu \gamma_\mu \partial_\mu) \psi(\mathbf{r}_\parallel)$ , where  $(\bar{v}_1, \bar{v}_2) = (c_x, c_y)$  and  $(\gamma_1, \gamma_2) = (\sigma_2, -\sigma_1)$ . Hence, the low-energy physics in the nematic phase is governed by Majorana fermions bound to the surface. We notice that in rapidly rotating neutron stars, the Majorana fermions also exist in the cores of quantized vortices.

The Majorana condition,  $\psi_\uparrow = i\psi_\downarrow^\dagger$ , indicates that the gapless surface states possess the Ising spin,  $\mathbf{S} \equiv [\psi_a^\dagger \sigma_{ab} \psi_b - \psi_a \sigma_{ab}^\text{T} \psi_b^\dagger]/4 = (0, 0, S)$ . Only perturbation which generates an effective mass in  $\mathcal{H}_{\text{surf}}$  is an external potential coupled to the Ising spin,  $\mathcal{H}_{\text{mass}} = M \int d^2\mathbf{r}_\parallel \bar{\psi}(\mathbf{r}_\parallel) (\sigma \cdot \hat{\mathbf{z}}) \psi(\mathbf{r}_\parallel)$ . Let us now capture the role of symmetry behind the Ising spin and mass acquisition of surface Majorana fermions. The key ingredient is the combined symmetry defined as  $P_3 \equiv \mathcal{T}C_{2,z}\tau_z$ . In the nematic phase, the  $C_2$  rotation about  $\hat{\mathbf{z}}$  denoted by  $C_{2,z} = -i\sigma_z$  only changes  $\mathbf{H}$  to  $(-H_x, -H_y, H_z)$ . This can be compensated by the TRS,  $\mathcal{T}$ , when  $\hat{\mathbf{H}} \cdot \hat{\mathbf{z}} = 0$ . Hence, the operator transforms the BdG Hamiltonian as  $P_3 \mathcal{H}(\mathbf{k}) P_3 = \mathcal{H}(\mathbf{k}) + \gamma \hbar \mathbf{H} \sigma \cdot \hat{\mathbf{z}}$ , where  $\mathbf{k} \equiv \mathbf{k} - 2(\mathbf{k} \cdot \hat{\mathbf{z}})\hat{\mathbf{z}}$  denotes the momentum transferred by  $P_3$ . Combining it with the PHS, one obtains the chiral symmetry,  $\{\Gamma, \mathcal{H}(0, 0, k_z)\} = 0$ , where  $\Gamma \equiv \mathcal{C}P_3$ . Similar to Eq. (7),  $w_{1d}$  is therefore well-defined along the chiral symmetric momenta  $\mathbf{k} = (0, 0, k_z)$ , and is estimated as  $w_{1d} = 2$  for  $\gamma \hbar H < E_F$  when  $\mathbf{H} \perp \hat{\mathbf{z}}$ .

As shown in Fig. 3(a), the surface Majorana fermion acquires the mass only when  $\mathbf{H}$  breaks the  $P_3$  symmetry. We plot the surface magnetization in Fig. 3(b). Owing to the Ising anisotropy, the gapless surface states which survive in  $\mathbf{H} \perp \hat{\mathbf{z}}$  do not contribute to the local magnetization density. In contrast, the massive Majorana fermions in  $\mathbf{H} \parallel \hat{\mathbf{z}}$  significantly enhances the surface magnetization. Since neutron stars possess strong axial

and toroidal magnetic fields, the Ising magnetic response gives rise to the anisotropic distribution of magnetization on the surface enclosing the  ${}^3P_2$  superfluid core.

*Conclusions.*— We have demonstrated that the low-energy structures of all  ${}^3P_2$  phases are governed by different types of topologically protected gapless fermionic excitations: Surface Majorana fermions in nematic phases and a quartet of itinerant Majorana fermions in the cyclic phase. The ferromagnetic phase is the same as  ${}^3\text{He-A}_1$  and is accompanied by a single itinerant Majorana fermion. The existence of topological fermions may significantly affect the heat transport and cooling mechanism through neutrino emission in the context of neutron stars. We also notice that the nematic and cyclic phases possess topological bosonic excitations.  ${}^3P_2$  superfluids offer a unique platform to study the interplay between non-abelian Majorana fermions and non-abelian fractional vortices [47, 65–67].

This work was supported by JSPS (No. JP16K05448 and No. JP25400268) and “Topological Materials Science” (No. JP15H05855) and “Nuclear Matter in Neutron Stars Investigated by Experiments and Astronomical Observations” (No. JP15H00841) KAKENHI on innovation areas from MEXT. The work of M. N. is also supported in part by the MEXT-Supported Program for the Strategic Research Foundation at Private Universities “Topological Science” (Grant No. S1511006).

- 
- [1] X.-L. Qi and S.-C. Zhang, *Rev. Mod. Phys.* **83**, 1057 (2011).
  - [2] Y. Ando, *Journal of the Physical Society of Japan* **82**, 102001 (2013).
  - [3] G. E. Volovik, *The Universe in a Helium Droplet* (Clarendon, Oxford, 2003).
  - [4] T. Mizushima, Y. Tsutsumi, T. Kawakami, M. Sato, M. Ichioka, and K. Machida, *J. Phys. Soc. Jpn.* **85**, 022001 (2016).
  - [5] T. Mizushima, Y. Tsutsumi, M. Sato, and K. Machida, *J. Phys.: Condens. Matter* **27**, 113203 (2015).
  - [6] Y. Tanaka, M. Sato, and N. Nagaosa, *J. Phys. Soc. Jpn.* **81**, 011013 (2012).
  - [7] M. Sato and S. Fujimoto, *J. Phys. Soc. Jpn.* **85**, 072001 (2016).
  - [8] A. P. Schnyder, S. Ryu, A. Furusaki, and A. W. W. Ludwig, *Phys. Rev. B* **78**, 195125 (2008).
  - [9] M. Sato, *Phys. Rev. B* **81**, 220504 (2010).
  - [10] A. P. Schnyder, P. M. R. Brydon, *J. Phys.: Condens. Matter* **27**, 243201 (2015).
  - [11] N. Read and D. Green, *Phys. Rev. B* **61**, 10267 (2000).
  - [12] D. A. Ivanov, *Phys. Rev. Lett.* **86**, 268 (2001).
  - [13] S. B. Chung and S.-C. Zhang, *Phys. Rev. Lett.* **103**, 235301 (2009).
  - [14] Y. Nagato, S. Higashitani, and K. Nagai, *Journal of the Physical Society of Japan* **78**, 123603 (2009).
  - [15] G. Volovik, *JETP Letters* **90**, 587 (2009), ISSN 0021-3640.
  - [16] T. Mizushima, M. Sato, and K. Machida, *Phys. Rev. Lett.* **109**, 165301 (2012).
  - [17] A. Kitaev, *Annals of Physics* **303**, 2 (2003), ISSN 0003-4916.
  - [18] C. Nayak, S. Simon, A. Stern, M. Freedman, and S. Das Sarma, *Rev. Mod. Phys.* **80**, 1083 (2008).
  - [19] G. E. Volovik and L. P. Gor’kov, *Zh. Eksp. Teor. Fiz.* **88**, 1412 (1985) [*Sov. Phys. JETP* **61**, 843 (1985)].
  - [20] M. Ozaki, K. Machida, and T. Ohmi, *Prog. Theor. Phys.* **74**, 221 (1985).
  - [21] M. Sigrist and K. Ueda, *Rev. Mod. Phys.* **63**, 239 (1991).
  - [22] G. Baym, C. J. Pethick, D. Pines, and M. Ruderman, *Nature* **224**, 879 (1969).
  - [23] D. Pines, J. Shaham, and M. Ruderman, *Nature Phys. Sci.* **237**, 83 (1972).
  - [24] T. Takatsuka and R. Tamagaki, *Prog. Theor. Phys.* **79**, 274 (1988).
  - [25] C. O. Heinke and W. C. G. Ho, *The Astrophysical Journal Letters* **719**, L167 (2010).
  - [26] D. Page, M. Prakash, J. M. Lattimer, and A. W. Steiner, *Phys. Rev. Lett.* **106**, 081101 (2011).
  - [27] D. G. Yakovlev, A. D. Kaminker, O. Y. Gnedin, and P. Haensel, *Phys. Rep.* **354**, 1 (2001).
  - [28] A. Y. Potekhin, J. A. Pons, and D. Page, *Space Sci. Rev.* **191**, 239 (2015).
  - [29] P. E. Reichley and G. S. Downs, *Nature* **234**, 48 (1971).
  - [30] P. W. Anderson and N. Itoh, *Nature* **256**, 25 (1975).
  - [31] R. Tamagaki, *Prog. Theor. Phys.* **44**, 905 (1970).
  - [32] M. Hoffberg, A. E. Glassgold, R. W. Richardson, and M. Ruderman, *Phys. Rev. Lett.* **24**, 775 (1970).
  - [33] T. Takatsuka and R. Tamagaki, *Prog. Theor. Phys.* **46**, 114 (1971).
  - [34] T. Takatsuka, *Prog. Theor. Phys.* **47**, 1062 (1972).
  - [35] T. Fujita and T. Tsuneto, *Prog. Theor. Phys.* **48**, 766 (1972).
  - [36] R. W. Richardson, *Phys. Rev. D* **5**, 1883 (1972).
  - [37] N. D. Mermin, *Phys. Rev. A* **9**, 868 (1974).
  - [38] J. A. Sauls and J. W. Serene, *Phys. Rev. D* **17**, 1524 (1978).
  - [39] Y. Li and C. Wu, *Sci. Rep.* **2**, 392 (2012).
  - [40] W. Yang, Y. Li, and C. Wu, *arXiv:1507.02768*.
  - [41] P. F. Bedaque, G. Rupak, and M. J. Savage, *Phys. Rev. C* **68**, 065802 (2003).
  - [42] L. B. Leinson, *Phys. Rev. C* **85**, 065502 (2012).
  - [43] P. F. Bedaque, A. N. Nicholson, and S. Sen, *Phys. Rev. C* **92**, 035809 (2015).
  - [44] P. Muzikar, J. A. Sauls, and J. W. Serene, *Phys. Rev. D* **21**, 1494 (1980).
  - [45] J. A. Sauls, D. L. Stein, and J. W. Serene, *Phys. Rev. D* **25**, 967 (1982).
  - [46] K. Masuda and M. Nitta, *Phys. Rev. C* **93**, 035804 (2016).
  - [47] K. Masuda and M. Nitta, *arXiv:1602.07050*.
  - [48] J. A. Sauls, Ph. D. thesis, S.U.N.Y. at Stony Brook (1980).
  - [49] D. Vollhardt and P. Wölfle, *The Superfluid Phases of Helium 3* (Taylor and Francis, London, 1990).
  - [50] See Supplemental Material at [URL will be inserted by publisher] for theoretical formulation.
  - [51] J. Serene and D. Rainer, *Phys. Rep.* **101**, 221 (1983).
  - [52] A. B. Vorontsov and J. A. Sauls, *Phys. Rev. B* **68**, 064508 (2003).
  - [53] T. Mizushima, *Phys. Rev. B* **86**, 094518 (2012).
  - [54] B. Paczynski, *Acta Astron.* **42**, 145 (1992).
  - [55] C. Thompson and R. C. Duncan, *MNRAS* **275**, 255

- (1995).
- [56] C. Thompson and R. C. Duncan, The Astrophysical Journal **473**, 322 (1996).
  - [57] A. Melatos, The Astrophysical Journal Letters **519**, L77 (1999).
  - [58] S.-O. Bäckman, C. G. Källman, and O. Sjöberg, Phys. Lett. **43B**, 263 (1973).
  - [59] S.-O. Bäckman, O. Sjöberg, and A. D. Jackson, Nucl. Phys. **A321**, 10 (1979).
  - [60] O. Sjöberg, Phys. Lett. **142B**, 229 (1984).
  - [61] S.-O. Bäckman, G.E. Brown, J.A. Niskanen, Phys. Rep. **124**, 1 (1985).
  - [62] V. Z. Vulovic and J. A. Sauls, Phys. Rev. D **29**, 2705 (1984).
  - [63] J. W. F. Venderbos, V. Kozii, and L. Fu, arXiv:1512.04554.
  - [64] M. Sato, Y. Tanaka, K. Yada, and T. Yokoyama, Phys. Rev. B **83**, 224511 (2011).
  - [65] G. W. Semenoﬀ and F. Zhou, Phys. Rev. Lett. **98**, 100401 (2007).
  - [66] M. Kobayashi, Y. Kawaguchi, M. Nitta, and M. Ueda, Phys. Rev. Lett. **103**, 115301 (2009).
  - [67] Y. Kawaguchi and M. Ueda, Physics Reports **520**, 253 (2012).

## Supplementary Material

### S1. Quasiclassical theory for $^3P_2$ superfluids

We here summarize the quasiclassical theory for  $^3P_2$  superfluids. The quasiclassical theory is the natural extension of the Landau's Fermi liquid theory to superfluid and superconducting phases. This theory covers vast scope of systems within the weak coupling regime  $k_F \xi \gg 1$ . This theory also offers a tractable way for studying the microscopic structure of spatially inhomogeneous superconductors and superfluids.

We start with the Hamiltonian for neutrons interacting through the potential  $\mathcal{V}_{a,b}^{c,d}$ ,

$$\begin{aligned} \mathcal{H} = & \int d\mathbf{r} \psi_a^\dagger(\mathbf{r}) \varepsilon_{ab} (-i\nabla) \psi_b(\mathbf{r}) \\ & + \frac{1}{2} \int d\mathbf{r}_1 \int d\mathbf{r}_2 \mathcal{V}_{a,b}^{c,d}(\mathbf{r}_{12}) \psi_a^\dagger(\mathbf{r}_1) \psi_b^\dagger(\mathbf{r}_2) \psi_c(\mathbf{r}_2) \psi_d(\mathbf{r}_1), \end{aligned} \quad (\text{S.1})$$

where  $\mathbf{r}_{12} \equiv \mathbf{r}_1 - \mathbf{r}_2$  denotes the relative coordinate and  $\psi_a$  and  $\psi_a^\dagger$  denote the fermionic field operators. The single-particle Hamiltonian density for neutrons under a magnetic field  $\mathbf{H}$  is given by

$$\varepsilon(\mathbf{k}) = \varepsilon_0(\mathbf{k}) - \frac{1}{2} \gamma \sigma_\mu H_\mu. \quad (\text{S.2})$$

The repeated Roman and Greek indices imply the sum over the spin degrees of freedom and  $(x, y, z)$ , respectively.

The central object of the theory is the propagator that contains both quasiparticles and superfluidity in equal footing. The quasiclassical propagator  $g(\hat{\mathbf{k}}, \mathbf{r}; \omega_n)$  is obtained from the Matsubara Green's function  $G(\mathbf{k}, \mathbf{r}; \omega_n)$  by integrating  $G$  over a shell  $v_F |k - k_F| < E_c \ll E_F$  [51]

$$g(\hat{\mathbf{k}}, \mathbf{r}; \omega_n) = \frac{1}{a} \int_{-E_c}^{+E_c} d\xi \tau_z G(\mathbf{k}, \mathbf{r}; \omega_n). \quad (\text{S.3})$$

The Matsubara Green's function is defined as

$$\begin{aligned} G(\mathbf{k}, \mathbf{r}; \omega_n) \equiv & - \int_0^\beta d\tau e^{i\omega_n \tau} \int d\mathbf{r}_{12} e^{-i\mathbf{k} \cdot \mathbf{r}_{12}} \\ & \times \langle \langle T_\tau [\Psi(\mathbf{r}_1, \tau) \bar{\Psi}(\mathbf{r}_2, 0)] \rangle \rangle \end{aligned} \quad (\text{S.4})$$

with  $\Psi = (\psi_\uparrow, \psi_\downarrow, \psi_\uparrow^\dagger, \psi_\downarrow^\dagger)^T$ ,  $\Psi(\tau) \equiv e^{\tau \mathcal{H}} \Psi e^{-\tau \mathcal{H}}$ , and the thermodynamic average  $\langle \langle \dots \rangle \rangle$ . The Matsubara Green's function is governed by the so-called Gor'kov equation. The normalization constant  $a$  corresponds to the weight of the quasiparticle pole in the spectral function.

The quasiclassical propagator  $g \equiv g(\hat{\mathbf{k}}, \mathbf{r}; \omega_n)$  is governed by the transport-like equation. Following the procedure in Ref. [51], one obtains the quasiclassical transport equation from the Gor'kov equation as

$$[i\omega_n \tau_z - v(\hat{\mathbf{k}}, \mathbf{r}) - \underline{\Delta}(\hat{\mathbf{k}}, \mathbf{r}), g] + i\mathbf{v}_F \cdot \nabla g = 0. \quad (\text{S.5})$$

The Fermi velocity is defined as  $\mathbf{v}_F(\hat{\mathbf{k}}) = \partial \varepsilon_0(\mathbf{k}) / \partial \mathbf{k}|_{\mathbf{k}=k_F \hat{\mathbf{k}}}$ . The term  $v$  in Eq. (S.5) consists of an external potential  $v_{\text{ext}}$  and quasiclassical self-energy  $\nu$  associated with Fermi liquid corrections, as  $v(\hat{\mathbf{k}}, \mathbf{r}) = v_{\text{ext}}(\mathbf{r}) + \nu(\hat{\mathbf{k}}, \mathbf{r})$ , where  $\nu = \text{diag}(\nu_0 + \sigma_\mu \nu_\mu, \bar{\nu}_0 + \sigma_\mu^T \bar{\nu}_\mu)$ . The external potential,  $\underline{v}(\hat{\mathbf{k}}, \mathbf{r})$ , is obtained with a magnetic Zeeman field as

$$\underline{v}(\hat{\mathbf{k}}, \mathbf{r}) = -\frac{1}{1 + F_0^a} \frac{1}{2} \gamma \hbar H_\mu \begin{pmatrix} \sigma_\mu & \\ & \sigma_\mu^T \end{pmatrix}, \quad (\text{S.6})$$

where  $F_0^a$  is the Fermi liquid parameter. The off-diagonal component of the quasiclassical self-energies is given as

$$\underline{\Delta}(\hat{\mathbf{k}}, \mathbf{r}) = \begin{pmatrix} \Delta(\hat{\mathbf{k}}, \mathbf{r}) & \\ \Delta^\dagger(-\hat{\mathbf{k}}, \mathbf{r}) & \end{pmatrix}. \quad (\text{S.7})$$

The quasiclassical transport equation (S.5) is a first-order ordinary differential equation along a trajectory in the direction of  $\mathbf{v}_F(\hat{\mathbf{k}})$ . The solution of the quasiclassical transport equation (S.5) is not uniquely determined per se, because  $a + bg$  satisfies the same equation as  $g$  ( $a$  and  $b$  are arbitrary constants). To obtain a unique solution for  $g$ , Eq. (S.5) must be supplemented by the normalization condition on the quasiclassical propagator as

$$[g(\hat{\mathbf{k}}, \mathbf{r}; \omega_n)]^2 = -\pi^2. \quad (\text{S.8})$$

The quasiclassical propagator  $\underline{g}$  that is a  $4 \times 4$  matrix in particle-hole and spin spaces is parameterized with spin Pauli matrices  $\sigma_\mu$  as

$$\underline{g} = \begin{pmatrix} g_0 + \sigma_\mu g_\mu & i\sigma_y f_0 + i\sigma_\mu \sigma_y f_\mu \\ i\sigma_y \bar{f}_0 + i\sigma_y \sigma_\mu \bar{f}_\mu & \bar{g}_0 + \sigma_\mu^T \bar{g}_\mu \end{pmatrix}. \quad (\text{S.9})$$

Here,  $\sigma_\mu^T$  denotes the transpose of the Pauli matrices  $\sigma_\mu$ . The off-diagonal propagators are composed of spin-singlet and triplet Cooper pair amplitudes,  $f_0$  and  $f_\mu$ . The quasiclassical propagators must satisfy the following relations arising from the Fermi statistics,  $[g(\hat{\mathbf{k}}, \mathbf{r}; \omega_n)]^\dagger = \tau_z g(\hat{\mathbf{k}}, \mathbf{r}; -\omega_n) \tau_z$  and  $[g(\hat{\mathbf{k}}, \mathbf{r}; \omega_n)]^T = \tau_y g(-\hat{\mathbf{k}}, \mathbf{r}; -\omega_n) \tau_y$ . From the normalization condition in Eq. (S.8), one obtains the relation,  $\bar{g}_0(\hat{\mathbf{k}}, \mathbf{r}; \omega_n) = -g_0(\hat{\mathbf{k}}, \mathbf{r}; \omega_n)$ . The diagonal propagator with analytic continuation  $i\omega_n \rightarrow E + i0_+$  defines the  $\mathbf{k}$ -resolved local density of states,

$$\mathcal{N}(\hat{\mathbf{k}}, \mathbf{r}; E) = -\frac{\mathcal{N}_F}{\pi} \text{Im} g_0(\hat{\mathbf{k}}, \mathbf{r}; \omega_n \rightarrow -iE + 0_+), \quad (\text{S.10})$$

where  $\mathcal{N}_F = \int \frac{d\mathbf{k}}{(2\pi)^3 |\mathbf{v}_F(\hat{\mathbf{k}})|}$  is the total density of states at the Fermi surface in the normal state.

The complete set of the self-consistent quasiclassical theory is composed of the transport equation (S.5) with the normalization condition in Eq. (S.8) in addition to



the Fermi liquid corrections and the gap equation. The diagonal self-energies associated with the Fermi liquid corrections are determined as

$$\nu_0(\hat{\mathbf{k}}, \mathbf{r}) = \sum_{\ell} A_{\ell}^{(s)} T \sum_n \left\langle P_{\ell}(\hat{\mathbf{k}} \cdot \hat{\mathbf{k}}') g_0(\hat{\mathbf{k}}', \mathbf{r}; \omega_n) \right\rangle_{\hat{\mathbf{k}}'}, \quad (\text{S.11})$$

$$\nu_{\mu}(\hat{\mathbf{k}}, \mathbf{r}) = \sum_{\ell} A_{\ell}^{(a)} T \sum_n \left\langle P_{\ell}(\hat{\mathbf{k}} \cdot \hat{\mathbf{k}}') g_{\mu}(\hat{\mathbf{k}}', \mathbf{r}; \omega_n) \right\rangle_{\hat{\mathbf{k}}'}, \quad (\text{S.12})$$

where  $P_{\ell}(x)$  is the Legendre polynomials with  $\ell = 0, 1, 2, \dots$  and  $\sum_n$  denotes the Matsubara sum with the cutoff energy  $E_c$ . The gap function is determined by the anomalous propagators as

$$\Delta_{ab}(\hat{\mathbf{k}}, \mathbf{r}) = T \sum_n \left\langle \mathcal{V}_{ab}^{cd}(\hat{\mathbf{k}}, \hat{\mathbf{k}}') \left[ i\sigma_{\mu}\sigma_y f_{\mu}(\hat{\mathbf{k}}', \mathbf{r}; \omega_n) \right]_{cd} \right\rangle_{\hat{\mathbf{k}}'}. \quad (\text{S.13})$$

The coefficients  $A_{\ell}^{(s)}$  and  $A_{\ell}^{(a)}$  are symmetric and antisymmetric quasiparticle scattering amplitudes, respectively, which are parametrized with the Landau's Fermi-liquid parameters  $F_{\ell}^{(s,a)}$  as  $A_{\ell}^{(s,a)} = F_{\ell}^{(s,a)} / [1 + F_{\ell}^{(s,a)} / (2\ell + 1)]$ .  $F_{\ell=1}^s$  and  $F_{\ell=0}^a$  give Fermi liquid corrections to the effective mass and spin susceptibility. In this paper, we use the following abbreviation for the average over the Fermi surface,  $\langle \dots \rangle_{\hat{\mathbf{k}}} = \frac{1}{N_F} \int \frac{d\mathbf{k}}{(2\pi)^3 |v_F(\mathbf{k})|} \dots$ .

In general, the order parameter of spin-triplet superfluids and superconductors,  $\Delta(\mathbf{k})$ , is parameterized with the rank 2 tensor  $d_{\mu i}$  as  $\Delta(\mathbf{k}) = i\sigma_{\mu}\sigma_y d_{\mu i} \hat{k}_i$ , where the former (latter) index denotes the spin (orbital) degrees of freedom of the Cooper pair. The rank 2 tensor is expressed in terms of the scalar function  $E \equiv \text{tr}(d)/3$ , the antisymmetric matrix  $A_{\mu i}$ , and the symmetric traceless matrix  $B_{\mu i}$  as

$$d_{\mu i} = E\delta_{\mu,i} + A_{\mu i} + B_{\mu i}. \quad (\text{S.14})$$

The antisymmetric matrix is defined as  $A_{\mu i} = (d_{\mu i} - d_{i\mu})/2$ , and the symmetric traceless matrix is given as  $B_{\mu i} = (d_{\mu i} + d_{i\mu})/2 - \delta_{\mu,i}E$ . The number of independent components in Eq. (S.14) is then given as  $3 \times 3 = 1 + 3 + 5$ , where the number in the right-hand side implies the multiplicities of eigenstates of the total angular momentum  $J = 0, 1, 2$ , respectively.

In dense neutron matter, the effective pairing interaction between neutrons drastically changes at the critical density  $\sim 10^{14}$  g/cm<sup>3</sup> [31]. In the lower densities  $\lesssim 10^{14}$  g/cm<sup>3</sup>, the  $^1S_0$  channel dominates the pairing interaction, which leads to the  $^1S_0$  superfluids of neutrons. In the higher density regime  $\gtrsim 10^{14}$  g/cm<sup>3</sup>, a repulsive core appears in the  $^1S_0$  channel, whereas the  $^3P_J$  ( $J = 0, 1, 2$ ) channels become important for the pairing interaction. Owing to the short-range negative spin-orbit force, the  $^3P_2$  channel becomes strong, whereas the  $^3P_0$

and  $^3P_1$  channels are repulsive at high densities. Hence, the transition from  $^1S_0$  to  $^3P_2$  superfluids take place at the critical density which is relevant for the interior density of neutron stars.

We here take only the short-range negative part of the  $^3P_2$  channel as the effective pairing interaction for dense neutrons. The interaction potential,  $\mathcal{V}_{a,b}^{c,d}(\mathbf{k}, \mathbf{k}') = \int d\mathbf{r}_{12} e^{-i(\mathbf{k}-\mathbf{k}') \cdot \mathbf{r}_{12}} \mathcal{V}_{a,b}^{c,d}(\mathbf{r}_{12})$ , is then expressed as the separable form of the  $^3P_2$  interaction channel,

$$\mathcal{V}_{a,b}^{c,d}(\hat{\mathbf{k}}, \hat{\mathbf{k}}') = g t_{\mu\nu,ab}(\hat{\mathbf{k}}) t_{\mu\nu,cd}^*(\hat{\mathbf{k}}), \quad (\text{S.15})$$

where  $g < 0$  denotes the coupling constant of the zero-range  $^3P_2$  interaction.  $^3P_2$  interaction channel is represented by the traceless symmetric tensor  $t_{\mu\nu}(\hat{\mathbf{k}})$  as [36]

$$t_{\mu\nu}(\hat{\mathbf{k}}) = \frac{1}{2\sqrt{2}} \left( \sigma_{\mu}\sigma_y \hat{k}_{\nu} + \sigma_{\nu}\sigma_y \hat{k}_{\mu} \right) - \frac{1}{3\sqrt{2}} \delta_{\mu\nu} \sigma_{\eta}\sigma_y \hat{k}_{\eta}, \quad (\text{S.16})$$

which obeys  $t_{\mu\nu}(\hat{\mathbf{k}}) = t_{\nu\mu}(\hat{\mathbf{k}})$  and  $\text{tr}[t] = 0$ . Substituting the separable form of the pairing interaction in Eq. (S.15) into Eq. (S.13), the pair potential is projected onto the  $^3P_2$  subsector as

$$\Delta(\mathbf{k}, \mathbf{r}) = i\sigma_{\mu}\sigma_y d_{\mu\nu} \hat{k}_{\nu} = \Delta_{\mu\nu}(\mathbf{r}) t_{\mu\nu}(\hat{\mathbf{k}}). \quad (\text{S.17})$$

Each component of the  $^3P_2$  pair potential is obtained from the anomalous propagator as

$$\begin{aligned} \Delta_{\mu\nu}(\mathbf{r}) &= ig \left\langle \text{tr} [t_{\mu\nu} \sigma_{\eta} \sigma_y] f_{\eta}(\hat{\mathbf{k}}', \mathbf{r}; \omega_n) \right\rangle \\ &= i \frac{g}{\sqrt{2}} T \sum_n \left\langle \hat{k}_{\nu} f_{\mu} + \hat{k}_{\mu} f_{\nu} - \frac{2}{3} \delta_{\mu\nu} \hat{k}_{\eta} f_{\eta} \right\rangle_{\hat{\mathbf{k}}}, \end{aligned} \quad (\text{S.18})$$

where  $\text{tr}_2(A) = \sum_a A_{aa}$ . The order parameter tensor  $d_{\mu\nu}$  is then determined by solving the gap equation

$$d_{\mu i}(\mathbf{r}) = \frac{g}{2} [\mathcal{F}_{\mu i}(\mathbf{r}) + \mathcal{F}_{i\mu}(\mathbf{r})] - \frac{g}{3} \delta_{\mu i} \text{tr}[\mathcal{F}(\mathbf{r})], \quad (\text{S.19})$$

with

$$\mathcal{F}_{\mu i}(\mathbf{r}) \equiv T \sum_n \left\langle f_{\mu}(\hat{\mathbf{k}}, \mathbf{r}; \omega_n) \hat{k}_i \right\rangle_{\hat{\mathbf{k}}}. \quad (\text{S.20})$$

The coupling constant is determined by the transition temperature  $T_{c0}$  in the absence of external fields as

$$\frac{1}{g} = \frac{\pi T_{c0}}{3} \sum_{|\omega_n| < \omega_c} \frac{1}{|\omega_{n,c}|} \quad (\text{S.21})$$

which is obtained from the linearized gap equation at  $T = T_{c0}$  with  $\omega_{n,c} = (2n + 1)\pi T_{c0}$  and the superfluid critical temperature at zero fields,  $T_{c0}$ .

## S2. Thermodynamics and surface structure in the weak coupling limit



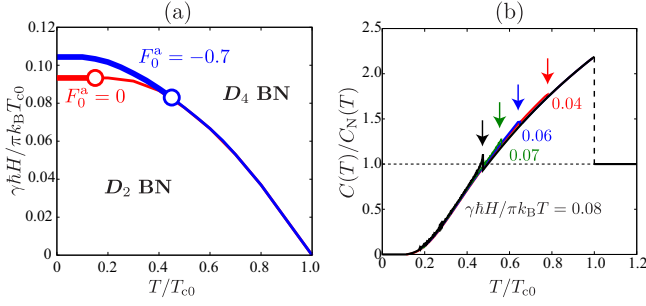


FIG. S1: (a) Phase diagram in the  $T$ - $H$  plane for  $F_0^a = -0.7$  and 0. The thick (thin) solid curve denotes the first- (second-) order phase transition line and these two lines meet at the tricritical point (circle). (b) Temperature dependence of the heat capacity  $C(T)/C_N(T)$  for fixed magnetic fields, where  $C_N(T)$  denotes the heat capacity in the normal state.

In the weak coupling limit, the thermodynamics of superfluid phases is determined by the Luttinger-Ward thermodynamic potential within the quasiclassical approximation [52, 53],

$$\delta\Omega[g] = \frac{1}{2} \int_0^1 d\lambda \text{Sp}' \left\{ (\underline{\mathcal{L}} + \underline{\Delta}) \left( g_\lambda - \frac{1}{2} g \right) \right\}, \quad (\text{S.22})$$

which describes thermodynamic potential relative to that in the normal state,  $\delta\Omega = \Omega_S - \Omega_N$ . We here set  $\text{Sp}'\{\dots\} \equiv \mathcal{N}_F T \sum_n \int d\mathbf{r} \int \frac{d\mathbf{k}}{4\pi} \dots$ . The quasiclassical auxiliary function  $g_\lambda$  is given by replacing  $\underline{\mathcal{L}} \mapsto \lambda \underline{\mathcal{L}}$  and  $\underline{\Delta} \mapsto \lambda \underline{\Delta}$  in (S.5).

In Fig. S1(a), we present the phase diagram in the  $T$ - $H$  plane for the Fermi liquid parameter,  $F_0^a = -0.7$  and 0. The lower magnetic field region is occupied by the  $D_2$  biaxial nematic phase. The phase undergoes the first (second) order phase transition to the  $D_4$  biaxial nematic phase in low (high) temperatures. The tricritical point at which the first and second order boundaries meet is sensitive to the Fermi liquid parameter  $F_0^a$ . As mentioned in the main text, the first order phase transition is attributed to the difference of the magnetic response between the  $D_2$  and  $D_4$  biaxial nematic phases.

In order to capture the consequence of the tricritical point, we plot the temperature dependence of the heat capacity,  $C(T)$ , in Fig. S1(b) under fixed magnetic fields. The heat capacity contains critical information on the thermal evolution of neutron stars [27]. The heat capacity in the superfluid state per volume is defined with the Luttinger-Ward thermodynamic potential,  $\delta\Omega$ , as

$$C_S(T) = C_N(T) - T \left( \frac{\partial^2 \delta\Omega}{\partial T^2} \right), \quad (\text{S.23})$$

where the heat capacity of the normal neutrons is given by  $C_N(T) = \frac{2\pi^2}{3} \mathcal{N}_F k_B^2 T$ . It is seen that the jump in the heat capacity increases as the magnetic field approaches the tricritical point.

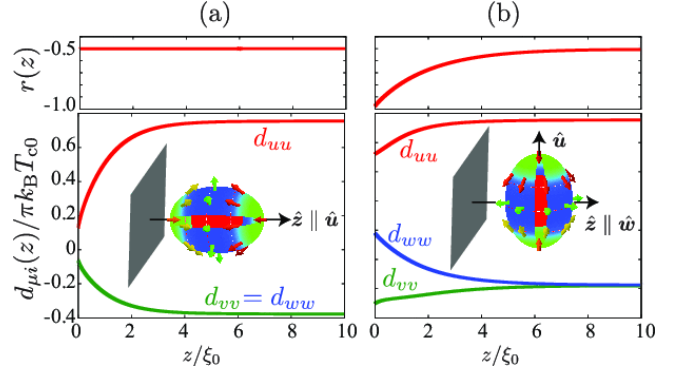


FIG. S2: Spatial profiles of order parameters,  $r(z)$  and  $d_{\mu i}(z)$ , in the nematic phase: (a)  $\hat{u} \parallel \hat{z}$  and (b)  $\hat{u} \perp \hat{z}$ , where the surface is normal to  $\hat{z}$  and  $z$  denotes the distance from the surface. The order parameter components are defined as  $d_{uu} \equiv \hat{u}_\mu d_{\mu i} \hat{u}_i$ ,  $d_{vv} \equiv \hat{v}_\mu d_{\mu i} \hat{v}_i$ , and  $d_{ww} \equiv \hat{w}_\mu d_{\mu i} \hat{w}_i$ .

Let us now consider a system having a specular surface at  $\mathbf{r} = \mathbf{r}_{\text{surf}} = (x, y, 0)$ , where  $z$  denotes the distance from the surface. In neutron stars, the surface may appear as the interface between the inner core and outer crust. A quasiparticle incoming to the surface along the trajectory of  $\mathbf{k}$  is specularly scattered by the wall to the quasiparticle state with

$$\underline{\mathbf{k}} = \mathbf{k} - 2\hat{\mathbf{s}}(\hat{\mathbf{s}} \cdot \mathbf{k}), \quad (\text{S.24})$$

where  $\hat{\mathbf{s}}$  denotes the unit vector pointing to the surface normal direction. The surface boundary condition on the  $4 \times 4$  quasiclassical propagator  $g(\hat{\mathbf{k}}, \mathbf{r}; \omega_n)$  is given by

$$g(\hat{\mathbf{k}}, \mathbf{r}_{\text{surf}}; \omega_n) = g(\underline{\hat{\mathbf{k}}}, \mathbf{r}_{\text{surf}}; \omega_n). \quad (\text{S.25})$$

The quasiclassical transport equation (S.5) subject to the normalization condition is generally mapped onto the Riccati-type differential equation by using the projection operator. For quasiparticle momentum  $\hat{\mathbf{k}}$ , the Riccati equation is numerically stable along the quasiclassical forward ( $\hat{\mathbf{k}}$ ) or backward ( $-\hat{\mathbf{k}}$ ) trajectory with an arbitrary initial value. The numerical integration of one-dimensional Riccati equations is performed with the fourth-order Runge-Kutta method.

In Fig. , we plot the spatial profiles of order parameters,  $r(z)$  and  $d_{\mu i}(z)$ , in the nematic phase. For simplicity, we ignore the magnetic Zeeman field and impose the following boundary condition on the tensor order parameter,

$$d_{\mu i}(x, y, z = \infty) = \Delta(T) \left( \hat{u}_\mu \hat{u}_i - \frac{1}{2} \hat{v}_\mu \hat{v}_i - \frac{1}{2} \hat{w}_\mu \hat{w}_i \right), \quad (\text{S.26})$$

which corresponds the uniaxial nematic phase with  $r(z = \infty) = -1/2$ .

Since the uniaxial nematic phase maintains the  $H = D_\infty \simeq O(2)$  symmetry, the order parameter manifold

is expressed by the broken symmetry,  $G/H = \text{U}(1) \times [\text{SO}(3)/\text{O}(2)]$ . As a consequence of the broken symmetry, the surface structure of the order parameter depends on the orientation of the triad  $(\hat{\mathbf{u}}, \hat{\mathbf{v}}, \hat{\mathbf{w}})$  with respect to the surface normal axis  $\hat{\mathbf{z}}$ . The surface structure in the case of  $\hat{\mathbf{u}} \parallel \hat{\mathbf{z}}$  is displayed in Fig. (a). the uniaxial nematic phase with  $r(z) = -1/2$  is maintained, whereas the amplitude of  $d_{\mu i}$  decays in the vicinity of the surface. In contrast, in the case of  $\hat{\mathbf{w}} \perp \hat{\mathbf{z}}$  shown in Fig. (b),  $r(z)$  smoothly changes from  $-1/2$  (uniaxial nematic phase) to  $-1$  ( $D_4$  biaxial nematic phase) and the biaxial nematic phase appears in the vicinity of the surface.

It turns out that the orientation dependence of the surface structure is understandable with the  $^3P_2$  constraint on the order parameter and the remaining symmetry. The order parameter orientation of  $\hat{\mathbf{u}} \parallel \hat{\mathbf{z}}$  preserves the  $\text{SO}(2)$  symmetry which is the simultaneous rotation of the spin and orbital spaces about the  $\hat{\mathbf{u}}$  axis. The rotational symmetry prohibits the appearance of the off-diagonal component of  $d_{\mu i}$ . In addition, as the order parameter approaches the surface, the pair breaking occurs in the order parameter component perpendicular to the surface,  $d_{uu} \equiv \hat{u}_\mu d_{\mu i} \hat{u}_i$ . The other components,  $d_{vv} \equiv \hat{v}_\mu d_{\mu i} \hat{v}_i$  and  $d_{ww} \equiv \hat{w}_\mu d_{\mu i} \hat{w}_i$ , must follow the spatial profile of  $d_{uu}$  so as to satisfy the  $^3P_2$  constraint, that is,  $\text{tr}(d) = 0$ . Hence, the case of  $\hat{\mathbf{u}} \parallel \hat{\mathbf{z}}$  preserves the symmetry of the uniaxial nematic phase but loses the condensation energy in the vicinity of the surface.

### S3. Effective Hamiltonian of cyclic phase

We here derive Eqs. (5) and (6) in the main text, which describe the effective low-energy Hamiltonian for the cyclic phase. We start to introduce the new Cartesian triad  $(\hat{\mathbf{e}}_1, \hat{\mathbf{e}}_2, \hat{\mathbf{e}}_3)$ , where  $\hat{\mathbf{e}}_3 \equiv \hat{\mathbf{e}}_1 \times \hat{\mathbf{e}}_2$  denotes the nodal direction  $\mathbf{k}_{q,\alpha}$ , as shown in Fig. 2(a) in the main text. In this basis, the cyclic order parameter,  $d_{\mu i} = \Delta(\hat{u}_\mu \hat{u}_i + e^{2\pi i/3} \hat{v}_\mu \hat{v}_i + e^{4\pi i/3} \hat{w}_\mu \hat{w}_i)$ , is recast into the linear combination of the eigenstates of  $M_J = -2$  and  $M_J = 1$  as

$$d_{\mu i} = \bar{\Delta}[\hat{e}_-^\mu \hat{e}_-^i - (\hat{e}_3^\mu \hat{e}_+^i + \hat{e}_+^\mu \hat{e}_3^i)], \quad (\text{S.27})$$

where  $\hat{\mathbf{e}}_\pm = (\hat{\mathbf{e}}_1 \pm i\hat{\mathbf{e}}_2)/\sqrt{2}$  and  $\bar{\Delta} \equiv \Delta\omega^2$ . For the case that the term,  $\hat{e}_3^\mu \hat{e}_+^i$ , is neglected, the  $4 \times 4$  BdG Hamiltonian density is then decomposed into a pair of  $2 \times 2$  matrix,  $\mathcal{H}_\pm(\mathbf{k})$ , as

$$\mathcal{H}(\mathbf{k}) \approx \begin{pmatrix} \mathcal{H}_+(\mathbf{k}) & \\ & \mathcal{H}_-(\mathbf{k}) \end{pmatrix}. \quad (\text{S.28})$$

The  $2 \times 2$  matrices are given as

$$\mathcal{H}_+(\mathbf{k}) = \varepsilon_0(\mathbf{k})\tau_3 + \sqrt{2}\hat{k}_3\bar{\Delta}\tau_1, \quad (\text{S.29})$$

$$\mathcal{H}_-(\mathbf{k}) = \varepsilon_0(\mathbf{k})\tau_3 + \bar{\Delta}\hat{k}_1\tau_1 + \bar{\Delta}\hat{k}_2\tau_2, \quad (\text{S.30})$$

where  $\mathbf{k} = k_1\hat{\mathbf{e}}_1 + k_2\hat{\mathbf{e}}_2 + k_3\hat{\mathbf{e}}_3$ . The mixing of  $\mathcal{H}_+(\mathbf{k})$  and  $\mathcal{H}_-(\mathbf{k})$  branches is found to be in the order of  $k^2$ .

Let  $V_{q,\alpha}$  be the small region around the Weyl point  $\mathbf{k}_{q,\alpha}$ . The lower energy in  $V_{q,\alpha}$  is then governed by  $\mathcal{H}_-$  with the  $M_J = -2$  contribution,  $\bar{\Delta}\hat{e}_-^\mu \hat{e}_-^i$ , while the  $\bar{\Delta}\hat{e}_+^\mu \hat{e}_+^i$  term is responsible for the upper branch  $\mathcal{H}_+$ . The  $\bar{\Delta}\hat{e}_3^\mu \hat{e}_+^i$  term brings about higher order corrections on  $k$ . To this end, the low-energy structure of the cyclic phase is given by the Hamiltonian,

$$\mathcal{H}_- = \sum_{q,\alpha} \sum_{\mathbf{k} \in V_{q,\alpha}} \mathbf{c}_\alpha^\dagger(\mathbf{k}) \mathcal{H}_-^{q,\alpha}(\mathbf{k}) \mathbf{c}_\alpha(\mathbf{k}), \quad (\text{S.31})$$

for the Weyl-type Bogoliubov quasiparticles with a single pseudospin species,

$$\mathcal{H}_-^{q,\alpha}(\mathbf{k}) = g_{\mu i} \tau_\mu (k_i - qA_i), \quad (\text{S.32})$$

where  $g_{\mu i} = \text{diag}(\bar{\Delta}/k_F, \bar{\Delta}/k_F, qv_F)$  and  $\mathbf{c}_\alpha(\mathbf{k}) = [c_\alpha(\mathbf{k}), c_\alpha^\dagger(-\mathbf{k})]^T$ . This describes the Weyl fermion with the effective electric charge  $q$  coupled to the effective gauge field  $\mathbf{A} = \mathbf{k}_{q,\alpha}/q$ . Hence, the eight nodal points can be identified as the Weyl points which are topologically protected by the monopole charge  $q = \pm 1$ .

Owing to the PHS,  $\mathcal{C}\mathcal{H}_-^{q,\alpha}(\mathbf{k})\mathcal{C}^{-1} = -\mathcal{H}_-^{-q,\alpha}(-\mathbf{k})$ , a pair of the monopole ( $q = +1$ ) and anti-monopole ( $q = -1$ ) exists along  $\hat{\mathbf{e}}_3$ . Following Ref. [63], we introduce the coordinate centered on the Weyl point,  $\mathbf{K} \equiv \mathbf{k} - \mathbf{k}_{q,\alpha}$ . Then, the four-component real quantum field,  $\psi(\mathbf{r}) = \mathcal{C}\psi(\mathbf{r})$ , is constructed from a PHS pair of the single-species Weyl fermions as  $\psi_\alpha(\mathbf{r}) \equiv \sum_{\mathbf{K}} e^{i\mathbf{K} \cdot \mathbf{r}} \psi_\alpha(\mathbf{K})$  with  $[c_\alpha(\mathbf{K}), c_\alpha(\mathbf{K}), c_\alpha^\dagger(-\mathbf{K}), c_\alpha^\dagger(-\mathbf{K})]^T$ . The low energy Hamiltonian is then recast into the Majorana-type Hamiltonian

$$\mathcal{H}_- = \sum_{\alpha=1}^4 \int d^3\mathbf{r} \bar{\psi}_\alpha(\mathbf{r}) [-i\bar{g}_{\mu i} \gamma_\mu \partial_i] \psi_\alpha(\mathbf{r}), \quad (\text{S.33})$$

where we introduced  $\bar{g}_{\mu i} = \text{diag}(\bar{\Delta}/k_F, \bar{\Delta}/k_F, v_F)$ ,  $(\gamma_1, \gamma_2, \gamma_3) = (\mu_1\tau_1, \mu_1\tau_2, \mu_3)$ , and  $\bar{\psi} = (\tau_1\psi)^T$  with the Pauli matrices  $\mu_i$  labeled by  $q = \pm 1$ . Hence, the low energy structure of the cyclic phase is reduced to three-dimensional massless Majorana fermions. The Majorana fermion possesses pseudospin 1/2 associated with the pairwise Weyl points and forms a quartet  $(\psi_1, \dots, \psi_4)$  as a consequence of the tetrahedral point group symmetry.

### S4. Topology and surface Majorana fermions in nematic phases

We start to clarify the topological structure of the nematic phase at zero fields. These phases which have  $\mathcal{T}^2 = -1$  and  $\mathcal{C}^2 = +1$  are categorized to the class DIII in the topological table [8]. The  $4 \times 4$  matrix,  $\mathcal{H}(\mathbf{k})$ , subject to  $\mathcal{C}^2 = +1$  and  $\mathcal{T}^2 = -1$  is parameterized by the four-dimensional spinor  $\hat{\mathbf{m}} = (\hat{m}_1, \hat{m}_2, \hat{m}_3, \hat{m}_4) \in S^3$ , as  $\mathcal{H}(\mathbf{k}) = |E(\mathbf{k})| \sum_{j=1}^4 \hat{m}_j(\mathbf{k}) \gamma_j$ , where  $\gamma_j$  denotes the Dirac  $\gamma$  matrices which obey  $\{\gamma_i, \gamma_j\} = 2\delta_{ij}$ . This indicates that the spinor  $\hat{\mathbf{m}}(\mathbf{k})$  is a projector that maps

$\mathbf{k} \in S^3$  onto the spinor space  $\hat{\mathbf{m}} \in S^3$ . The topological invariant relevant to the homotopy group of the mapping,  $\pi_3(S^3) = \mathbb{Z}$ , is the winding number [4, 5],

$$w_{3d} = \int \frac{d^3\mathbf{k}}{12\pi^3} \epsilon_{\mu\nu\eta} \epsilon_{ijkl} \hat{m}_i \partial_{k_\mu} \hat{m}_j \partial_{k_\nu} \hat{m}_k \partial_{k_\eta} \hat{m}_l, \quad (\text{S.34})$$

which is estimated as  $w_{3d} = -1$  for  $r \neq -1$  ( $\mu, \nu, \eta = x, y, z$  and  $i, j, k, l = 1, \dots, 4$ ). Since  $w_{3d}$  characterizes the classes of topologically distinct  $\hat{\mathbf{m}}$ -configurations, the domains having different values of  $w_{3d}$  cannot be continuously connected to each others and gapless fermionic excitations emerge at the interface/surface. For the  $D_4$  BN phase at  $r = -1$ , the point nodes can be removed by adding a small perturbation that unchanges the symmetries. As pointed out in Ref. [9], however, an ambiguity in choosing the perturbation makes  $w_{3d}$  gauge-dependent. Only the parity of  $w_{3d}$  remains gauge-invariant. Hence, the  $D_4$  BN phase is topological since the  $\mathbb{Z}_2$  number is  $\nu = (-1)^{w_{3d}} = -1$ , while  $\nu = +1$  corresponds to a topologically trivial state. Hence, at zero fields, the nematic phases for all  $r$  possess topologically nontrivial structure, and thus are accompanied by gapless fermionic excitations.

The hallmark of the nontrivial topological structure in the class DIII is the presence of surface Majorana fermions. To unveil the existence of characteristic gapless surface states in the nematic phase, we here solve the Bogoliubov-de Gennes (BdG) equation,

$$\mathcal{H}(k_x, k_y, -i\partial_z)\varphi(\mathbf{r}) = E\varphi(\mathbf{r}), \quad (\text{S.35})$$

within the Andreev approximation. The surface is set to be normal to the  $z$  axis.

The Andreev equation is derived from the BdG equation by decomposing the quasiparticle wavefunction  $\varphi_i(\mathbf{r})$  to the slowly varying part  $\tilde{\varphi}$  and the rapid oscillation part with the Fermi wave length  $k_F^{-1}$ ,  $\varphi_i(\mathbf{r}) = \sum_{\alpha=\pm} C_\alpha \tilde{\varphi}_\alpha(\mathbf{r}) e^{ik_\alpha \cdot \mathbf{r}}$ .  $\mathbf{k}_\alpha$  denotes the momentum of incoming ( $\alpha = +$ ) and outgoing ( $\alpha = -$ ) quasiparticles. The rigid boundary condition at  $\mathbf{r} = \mathbf{r}_{\text{surf}}$ ,  $\varphi(\mathbf{r}_{\text{surf}}) = 0$ , leads to  $C_+ = -C_-$  and the continuity condition  $\tilde{\varphi}_+(\mathbf{r}_{\text{surf}}) = \tilde{\varphi}_-(\mathbf{r}_{\text{surf}})$ . The slowly varying function is governed the Andreev equation for  $\tilde{\varphi}_\alpha(\mathbf{r})$  as

$$\left[ -iv_F(\hat{\mathbf{k}}_\alpha) \cdot \nabla_{\mathcal{I}_z} + \underline{v} + \underline{\Delta}(\hat{\mathbf{k}}_\alpha, \mathbf{r}) \right] \tilde{\varphi}_\alpha(\mathbf{r}) = E\tilde{\varphi}_\alpha(\mathbf{r}). \quad (\text{S.36})$$

The normalization condition is imposed on  $\tilde{\varphi}_\alpha(\mathbf{r})$  as  $\sum_\alpha \int d\mathbf{r} \tilde{\varphi}_\alpha^\dagger(\mathbf{r}) \tilde{\varphi}_\alpha(\mathbf{r}) = 1$ . This Andreev approximation is valid in the weak-coupling regime,  $k_F \xi = 2E_F/\Delta \gg 1$ . In Eq. (S.36), we have introduced the  $4 \times 4$  matrix form of the pair potential,  $\underline{\Delta}(\hat{\mathbf{k}}, \mathbf{r})$ .

We parameterize the order parameter of the nematic phase as

$$d_{\mu\nu} = \Delta_0 \begin{pmatrix} f_1 & & \\ & f_2 & \\ & & -(f_1 + f_2) \end{pmatrix}. \quad (\text{S.37})$$

We set a specular surface to be normal to the  $\hat{z}$ -axis and the region  $z > 0$  is occupied by the nematic phase. We also suppose the spatially uniform isotropic energy gap  $\Delta$ . Using the unitary matrix  $S(\phi_{\mathbf{k}}) \equiv (\sigma_x + \sigma_z) e^{i\vartheta\sigma_z}/\sqrt{2}$  with  $\vartheta = \frac{\phi_{\mathbf{k}}}{2} - \frac{\pi}{4}$ , one finds that the pair potential can be transformed into the diagonal representation,

$$\Delta(\hat{\mathbf{k}}, \mathbf{r}) = \Delta S(\phi_{\mathbf{k}}) \begin{pmatrix} \hat{k}'_z + i\hat{k}'_{\parallel} & 0 \\ 0 & -\hat{k}'_z + i\hat{k}'_{\parallel} \end{pmatrix} S^T(\phi_{\mathbf{k}}), \quad (\text{S.38})$$

where we introduced the rescaled momentum  $(\hat{k}'_x, \hat{k}'_y, \hat{k}'_z) = (f_1 \hat{k}_x, f_2 \hat{k}_y, \hat{k}_z)$  and  $\hat{k}'_{\parallel} = \sqrt{\hat{k}'_x^2 + \hat{k}'_y^2}$ . By employing the unitary transformation, the pair potential for the nematic order parameter (S.37) reduces to the time-reversal-symmetric copy of chiral  $p$ -wave pairing. The bound state solution within  $|E(\mathbf{k}_{\parallel})| \leq \Delta$  therefore has the energy dispersion linear in the momentum  $\mathbf{k}_{\parallel} = (k_x, k_y)$  as

$$E_0(\mathbf{k}_{\parallel}) = \pm \sqrt{c_x^2 k_x^2 + c_y^2 k_y^2}. \quad (\text{S.39})$$

The velocities are

$$c_x = \frac{\Delta}{k_F} f_1, \quad c_y = \frac{\Delta}{k_F} f_2 \quad (\text{S.40})$$

The wavefunction for the positive energy branch is given by

$$\varphi_{0,\mathbf{k}_{\parallel}}^{(+)}(\mathbf{r}) = N_{\mathbf{k}} e^{i\mathbf{k}_{\parallel} \cdot \mathbf{r}_{\parallel}} f(k_{\perp}, z) (\Phi_+ - e^{i\phi_{\mathbf{k}}} \Phi_-), \quad (\text{S.41})$$

where  $N_{\mathbf{k}}$  is the normalization constant and  $\mathcal{U} \equiv \text{diag}(U, U^*)$ . The particle-hole symmetry ensures the one-to-one correspondence between the two branches of the energy eigenstates through  $\varphi_{0,\mathbf{k}_{\parallel}}^{(-)}(\mathbf{r}) = \mathcal{C} \varphi_{0,-\mathbf{k}_{\parallel}}^{(+)}(\mathbf{r})$ . In Eq. (S.41), we also set  $f(k_{\perp}, z) = \sin(k_{\perp} z) e^{-z/\xi}$  with  $k_{\perp}^2 \equiv k_F^2 - k_{\parallel}^2$ . The spinors,  $\Phi_+ \equiv (1, 0, 0, -i)^T$  and  $\Phi_- \equiv (0, i, 1, 0)^T$ , are the eigenvectors of the spin operator  $S_z \equiv \frac{1}{2} \text{diag}(\sigma_z, -\sigma_z^T)$  in the Nambu space,  $S_z \Phi_{\pm} = \pm \frac{1}{2} \Phi_{\pm}$ .

We now expand the quantized field  $\Psi = (\psi_{\uparrow}, \psi_{\downarrow}, \psi_{\uparrow}^{\dagger}, \psi_{\downarrow}^{\dagger})^T$  in terms of the positive energy states of the surface Andreev bound states. For low temperature regimes  $T \ll \Delta$ , the field operator can be constructed from the contributions of only the surface Andreev bound states as  $\Psi(\mathbf{r}) = \sum_{\mathbf{k}_{\parallel}} [\varphi_{0,\mathbf{k}_{\parallel}}^{(+)}(\mathbf{r}) \eta_{\mathbf{k}_{\parallel}} + \mathcal{C} \varphi_{0,\mathbf{k}_{\parallel}}^{(+)}(\mathbf{r}) \eta_{\mathbf{k}_{\parallel}}^{\dagger}]$ , where the continuum states with  $E > \Delta$  are omitted. Substituting Eq. (S.41) into the expansion form of  $\Psi$ , the quantized field operator contributed from the surface Andreev bound states obeys the so-called Majorana Ising condition

$$\psi_{\uparrow}(\mathbf{r}) = i\psi_{\downarrow}^{\dagger}(\mathbf{r}). \quad (\text{S.42})$$

The condition in Eq. (S.42) clarifies that the Majorana fields constructed from the surface Andreev bound states

reproduce the Ising spin property and the surface bound states are not coupled to the local density operators. Using Eq. (S.42), one first finds that the surface states do not contribute to the local density operator,

$$\rho^{(\text{surf})}(\mathbf{r}) = 0. \quad (\text{S.43})$$

The surface helical Majorana fermions can not be coupled to the local density fluctuation and thus are very robust against non-magnetic impurities. Similarly, the local spin operator is constructed from the surface Majorana fermion in Eq. (S.42) as

$$\mathbf{S}^{(\text{surf})} \parallel \hat{\mathbf{z}}. \quad (\text{S.44})$$

Equation (S.44) implies that only the  $S_z$  component is

nonzero while the other components are identically zero.

By using Eq. (S.42), the effective Hamiltonian for the surface Majorana fermion is given as,

$$\mathcal{H}_{\text{surf}} = \int d^2\mathbf{r}_{\parallel} \bar{\psi}(\mathbf{r}_{\parallel}) (-i\bar{v}_{\mu}\gamma_{\mu}\partial_{\mu})\psi(\mathbf{r}_{\parallel}), \quad (\text{S.45})$$

where  $(\bar{v}_1, \bar{v}_2) = (c_x, c_y)$  and  $(\gamma_1, \gamma_2) = (\sigma_2, -\sigma_1)$ . We also introduced the two-component spinor  $\psi = (\psi_{\uparrow}, \psi_{\downarrow})$  and  $\bar{\psi} = i(\sigma_1\psi)^T$ . Hence, the low-energy physics in the nematic phase is governed by Majorana fermions bound to the surface. We notice that in rapidly rotating neutron stars, the Majorana fermions also exist in the cores of quantized vortices.